

FREE VERSUS CONSTRAINED EVOLUTION OF THE 2+1 EQUIVARIANT WAVE MAP

RALF PETER AND JÖRG FRAUENDIENER

ABSTRACT. We compare the numerical solutions of the 2+1 equivariant Wave Map problem computed with the symplectic, constraint respecting Rattle algorithm and the well known fourth order Runge-Kutta method. We show the advantages of the Rattle algorithm for constrained system compared to the free evolution with the Runge-Kutta method. We also present an expression, which represents the energy loss due to constraint violation. Taking this expression into account we can achieve energy conservation for the Runge-Kutta scheme, which is better than with the Rattle method. Using the symplectic scheme with constraint enforcement we can reproduce previous calculations of the equivariant case without imposing the symmetry explicitly, thereby confirming that the critical behaviour is stable.

1. INTRODUCTION

Down to the present day, the use of symplectic, or more general geometric, numerical integration methods in the field of (general) relativistic (field) equations is not very common. To our knowledge the first work was done in [4] and [3] to solve ODEs in the context of cosmological space-times. The step to field equations was done in [27] and [28]. A symplectic integrator for post Newtonian equations was developed only recently [23]. A reason why this has not been done in the past very often, is the different symplectic structure of General Relativity compared to usual Hamiltonian systems [8].

Here, we want to present another contribution to the problem of solving relativistic field equations with the help of symplectic integrators. We compare the numerical solution of a 2+1 dimensional Wave Map system solved with a symplectic, constraint preserving (at least in a given accuracy) integration scheme with the standard fourth order Runge-Kutta method. We will show that we can reproduce the qualitative results gained by Bizoń et.al. [5] and Isenberg and Liebling [11] in the so called equivariant case.

The outline of this article is the following: in section 2 we give a brief description of the symplectic integration method, which we will use for our numerical studies. As already mentioned, we solve a Wave Map system to show the differences between the integration methods. So in section 3 we describe Wave Maps in general and concentrate then on the 2+1 equivariant case. In section 4 we derive a correction term for the energy, which is caused by the constraint violation during the numerical time evolution. The numerical setup, including the choice of the initial data and the boundary conditions are presented in section 5. Finally, in section 6, we present some results of our numerical studies.

Our numerical results can be put into three independent categories:

- (a) The comparison of the standard fourth order Runge-Kutta method with the Rattle method.
- (b) The correction of the energy by taking the constraint violation into account.
- (c) The blow up dynamics of the 2+1 equivariant Wave Map, where we reproduce known results.

2. THE RATTLE METHOD

The Rattle method is a numerical integration method for constrained ODE systems. It is a further development of the Shake algorithm [31] (which itself is based on the well known Störmer-Verlet method [9]) to take the presence of constraints into account. It was developed by Andersen [1] in the context of molecular

2010 *Mathematics Subject Classification.* 35L67, 35L70, 65M20, 65P10, 74H35.

We thank Christian Lubich for pointing out the Rattle method to us. RP was supported by a DAAD and a University of Otago Doctoral Scholarship. This research was partially funded by the Royal Society of New Zealand via the Marsden Fund.

dynamics. Later, it was shown by Leimkuhler and Skeel [22] that the Rattle method belongs to the group of the symplectic integrators.

Symplectic integrators are a certain class of geometric integrators [9, 10, 21, 24]. Their characteristic feature is the conservation of a geometric structure or quantity. Such quantities can be for example the energy, the momentum, the phase space volume or, like in the case of the symplectic integrators, the symplectic 2-form $\omega = dq^a \wedge dp_a$.

In many branches of physics and applied mathematics, including celestial mechanics, molecular dynamics and quantum mechanics symplectic integrators have been used very successfully for years. Very often the numerical results, especially in terms of long-term energy and (angular) momentum conservation, are much better compared to non-symplectic integrators [10].

Now we give a brief description of the Rattle method. For further details we refer to the original paper [1]. We consider a Lagrangian system with holonomic constraints ϕ^A and an action of the following form¹:

$$\mathcal{A}[q, \dot{q}, \lambda] = \int \left(\frac{1}{2} M_{kj} \dot{q}^k \dot{q}^j - V(q) + \lambda_A \phi^A(q) \right) dt$$

which leads to the Euler-Lagrange equations

$$(1) \quad \begin{aligned} \frac{d}{dt} (M_{jk} \dot{q}^k) + \partial_j V - \lambda_A \partial_j \phi^A &= 0, \\ \phi^A(q) &= 0. \end{aligned}$$

The constraint equation (1) implies also an additional constraint on the velocities:

$$\psi^A(q, \dot{q}) := \frac{d}{dt} \phi^A(q) = \dot{q}^j \partial_j \phi^A = 0.$$

With M we denote the mass matrix, with q the generalized coordinates, \dot{q} their corresponding velocities, λ_A are the Lagrangian multipliers and V is the potential. With the small Latin indices we label the dynamical variables and with the capital indices the constraints. We use here and throughout the whole article the common dot notation for time derivatives: $\dot{f} := \partial_t f$.

A time-step with the Rattle method starts with a Störmer-Verlet step using the unconstrained equations. In general the result does not satisfy the constraints. Therefore, the next step is to compute the appropriate amount of the constraint force $-\lambda_A \partial_j \phi^A$, which is necessary to push the estimated solution to the constraint surface. This is done by first correcting the coordinates q^j by iteratively solving the constraint $\phi^A = 0$ to determine the values of the Lagrange multipliers. Once these constraints are satisfied to a given accuracy the velocity constraints $\psi^A = 0$ are solved in a similar way to correct the velocities.

3. WAVE MAPS

Wave Maps are systems of generalized wave equations. They appear in several physical models, for example as nonlinear sigma models in particle physics [12] as well as the Einstein equations for a certain class of electro-vacuum space-times [2] or in cosmological models [29]. On the other hand, Wave Maps are of mathematical interest, because of their nonlinear structure and the possibility for singularity formation. Wave Maps are also the simplest example for geometric wave equations [32].

3.1. General. In general, a Wave Map describes a mapping from the $m + 1$ -dimensional Lorentzian manifold \mathcal{M} into a n -dimensional Riemannian manifold \mathcal{N} . Usually we distinguish between two different kinds of formulations for the Wave Maps. The first, so-called intrinsic formulation, describes the mapping directly from the base manifold \mathcal{M} into the target manifold \mathcal{N} .

$$\begin{aligned} \Theta: \mathcal{M} &\rightarrow \mathcal{N} \\ x &\mapsto \xi = \Theta(x). \end{aligned}$$

¹It is only possible for systems with holonomic constraints to write the action in this form.

We denote here and in the following the coordinates in \mathcal{M} with $x = (x^0, x^1, \dots, x^m)$ and with $\xi = (\xi^1, \dots, \xi^n)$ the coordinates in \mathcal{N} . Further, g_{ab} is the metric on \mathcal{M} and $h_{\beta\gamma}$ the metric on \mathcal{N} , so small Latin indices refer to manifold \mathcal{M} and small Greek indices to \mathcal{N} .

The action for the intrinsic formulation of the Wave Map is

$$\mathcal{A}[\Theta, \nabla\Theta] = \int_{\mathcal{M}} g^{ab} \nabla_a \Theta^\beta \nabla_b \Theta^\gamma h_{\beta\gamma} \sqrt{|g|} d^{m+1}x.$$

We denote with ∇_a the covariant derivative with respect to the metric g_{ab} on \mathcal{M} and with g the determinant of g_{ab} .

The variation of the action with respect to the field variables Θ^β gives us the equations of motion:

$$(2) \quad \square_g \Theta^\beta + \Gamma^\beta_{\mu\nu} \nabla^\mu \Theta^\nu = 0.$$

With $\square_g = \nabla^a \nabla_a$ we denote the d'Alembert operator (wave operator) on the base manifold \mathcal{M} and with $\Gamma^\beta_{\mu\nu} = \Gamma^\beta_{\mu\nu}(\Theta(x))$ the Christoffel symbols corresponding to the metric $h_{\beta\gamma}$ on \mathcal{N} . Equation (2) shows clearly that Wave Maps are generalizations of the wave equation ($\mathcal{N} = \mathbb{R}$) on the one side and the geodesic equation ($\mathcal{M} = \mathbb{R}$) on the other side.

A different way to describe Wave Maps is the so-called extrinsic formulation. In this formulation we assume the target manifold \mathcal{N} isometrically embedded into a higher dimensional euclidean space \mathbb{R}^p , $p > n$.

$$U : \mathcal{M} \rightarrow \mathcal{N} \hookrightarrow \mathbb{R}^p \\ x \mapsto z = U(x)$$

with $z = z^1, \dots, z^p$ the coordinates on \mathbb{R}^p and the notation for the variables in \mathcal{M} being the same as for the intrinsic formulation. In this case we need additional conditions $\phi(z) = 0$, which ensure that the image of the mapping lies in the sub-manifold \mathcal{N} of \mathbb{R}^p . We can do that by attaching the constraint expressions $\phi(z)$ to the action via Lagrangian multipliers. For the following purpose we can assume that it is enough that $p = n + 1$, which means that we need only one equation to describe the embedding of \mathcal{N} into \mathbb{R}^{n+1} . We write for the action of the extrinsic formulation

$$(3) \quad \mathcal{A}[U, \nabla U, \lambda] = \int_{\mathcal{M}} \left(g^{ab} \nabla_a U^A \nabla_b U^B \delta_{AB} + 2\lambda \phi \right) \sqrt{|g|} d^{m+1}x.$$

The capital Latin indices refer to \mathbb{R}^{n+1} and δ_{AB} denotes the Euclidean metric on \mathbb{R}^{n+1} .

Again, extremization of this action results in the equations of motion for this formulation:

$$\square_g U^A + \lambda \partial^A \phi = 0, \\ \phi(z) = 0.$$

3.2. 2+1 Wave Map. In the following we will concentrate on a Wave Map with the base manifold $\mathcal{M} = \mathbb{M}^{2+1}$, the 2 + 1 dimensional Minkowski space-time and the target manifold $\mathcal{N} = \mathbb{S}^2$, the 2-sphere.

Intrinsic Formulation. We will use the intrinsic formulation to discuss the basic properties of the 2+1 Wave Map. In this formulation, we write for the map:

$$\Theta : \mathbb{M}^{2+1} = \mathbb{R}^2 \times \mathbb{R} \rightarrow \mathbb{S}^2 \\ (x^0, x^1, x^2) \mapsto (\vartheta(x^0, x^1, x^2), \varphi(x^0, x^1, x^2)).$$

With the common notation for spherical coordinates on the 2-sphere we write for the line element

$$ds_{\mathbb{S}^2}^2 = d\vartheta^2 + \sin^2 \vartheta d\varphi^2.$$

The equations of motion take the following form:

$$(4) \quad \square_g \vartheta - \sin \vartheta \cos \vartheta \nabla^a \varphi \nabla_a \varphi = 0,$$

$$(5) \quad \square_g \varphi + 2 \cot \vartheta \nabla^a \vartheta \nabla_a \varphi = 0.$$

Further, we choose polar coordinates on the Minkowski space-time with the metric

$$ds_{\mathbb{M}^{2+1}}^2 = g_{ab} dx^a dx^b = dt^2 - dr^2 - r^2 d\sigma^2$$

where r is the radial and σ the angular coordinate. The most commonly studied situation for this Wave Map is the so-called equivariant case. In this case one sets $\vartheta(t, r, \sigma) = \vartheta(t, r)$ and $\varphi(t, r, \sigma) = \sigma$. The latter assumption means that the Wave Map maps rotations on Minkowski space around the origin to rotations of the sphere around the 3-axis with the same angle. In this case, the equation (5) is identically satisfied and (4) reduces to

$$(6) \quad \ddot{\vartheta} - \partial_{rr}\vartheta - \frac{1}{r}\partial_r\vartheta + \frac{\sin(2\vartheta)}{2r^2} = 0.$$

By confining to the equivariant case one needs to solve only one equation, but at the cost of having to deal with a coordinate singularity at $r = 0$. This equation together with the initial data

$$(7) \quad \vartheta(0, r) = \vartheta_0(r) \quad \text{and} \quad \dot{\vartheta}(0, r) = \vartheta_1(r)$$

is the Cauchy problem, which was studied in [5]. Equation (6) has two non-trivial, static solutions with $\vartheta(r) \in [0, \pi]$:

$$(8) \quad \vartheta_S(r) = 2\arctan(r^{\pm 1}).$$

The local well posedness of the Cauchy problem for Wave Maps with general target manifold, was proven in [13] and [15]. The study of the global well posedness started with the investigation of the equivariant case. This was done in [6, 7, 34–36]. The problem of global well-posedness for the non-symmetric 2+1 Wave Map with small initial data² was first addressed by Tataru [42]. Later work include [14, 33, 40, 41, 44]. For the case of a hyperbolic target manifold, see [16, 17]. Just recently the global well-posedness for the Cauchy problem in 2+1 dimensions for large energy initial data was first proven by Krieger and Schlag for the hyperbolic target [20] and by Sterbenz and Tataru for the \mathbb{S}^2 case [38, 39]. Finally, we want to recommend here the review article by Krieger [18] on the Wave Map problem which covers the most important results and references up to the year 2008.

The main interest in studying the Wave Map equations and particularly the 2+1 Wave Map into a 2-sphere is the formation of singularities. These question is closely related to the previously discussed problem of global well-posedness or regularity. In the 1+1 case it is easy to show that no singularities can form, because the Wave Map equations are equivalent to the standard 1+1 wave equation. For spatial dimensions larger than two it is known that the Wave Maps can form singularities. See [18, 43] for detailed information on this. Only for the 2+1 case it was for a long time not known. In 2001 Bizoń et. al. presented the first crucial numerical evidence for the singularity formation of the 2+1 dimensional Wave Map into the 2-sphere. We are going to present their results and point out the important contributions during the last years in this exciting field. Based on their numerical observations of the equivariant case Bizoń et. al. formulated three conjectures about the singularity formation:

Conjecture 1 (On blow-up for large data). *For initial data (7) with sufficiently large energy, the solutions of equation (6) blow up in finite time in the sense that the derivative $\partial_r\vartheta(t, 0)$ diverges as $t \nearrow T$ for some $T > 0$.*

Conjecture 2 (On blow-up profile). *Suppose that the solution $\vartheta(t, r)$ of the initial-value problem (6) and (7) blows up at some time $T > 0$. Then, there exists a positive function $s(t) \searrow 0$ for $t \nearrow T$ such that*

$$\lim_{t \nearrow T} \vartheta(t, s(t)r) = \vartheta_S(r)$$

This conjecture was proven by Struwe in [37], where, he not only proved the above statement, but further he showed that the existence of a non-trivial (non-constant) harmonic map is a necessary condition for a singularity formation. Struwe showed that the singularity formation appears as an energy concentration at the origin and the *bubbling-off of a harmonic map*. The latter is the decomposition of the solution near the blow up time T in the following form (see [19])

$$(9) \quad \vartheta(t, r) = \vartheta_S(s(t)r) + R(t, r).$$

The function $R(t, r)$ is a radiative term and $\vartheta_S(s(t)r)$ the rescaled static solution. The error term's local energy goes to zero as the time reaches the blow up time T . Equipped with the result in [37] Krieger,

²Small means here, small with respect to the energy. In other words, the energy is below a critical value.

Schlag and Tataru were able to construct the first blow up scenario for the 2+1 Wave Map into the 2-sphere [19]. This was later generalized to surfaces of revolution, which includes the 2-sphere, as target manifold.

Conjecture 3 (On energy concentration). *Suppose that the solution $\vartheta(t, r)$ of the initial-value problem (6) and (7) blows up at some time $T > 0$. Define the kinetic and the potential energies at time $t < T$ inside the past light-cone of the singularity by*

$$E_{kin}(t) = \pi \int_0^{T-t} \dot{\vartheta}^2 r \, dr \quad \text{and} \quad E_{pot}(t) = \pi \int_0^{T-t} \left[(\partial_r \vartheta)^2 + \frac{\sin^2 \vartheta}{r^2} \right] r \, dr$$

Then:

(a) *the kinetic energy tends to zero at the singularity*

$$\lim_{t \nearrow T} E_{kin}(t) = 0$$

(b) *the potential energy equal to the energy of the static solution ϑ_S concentrates at the singularity*

$$\lim_{t \nearrow T} E_{pot}(t) = E[\vartheta_S] = 4\pi.$$

The behaviour of the energy, as described in the last conjecture is a direct consequence of the splitting (9) if one considers the vanishing energy of the radiation term in the past light cone.

In a recent detailed study on the singularity formation Raphaël and Rodnianski constructed a stable blow up scenario [26]. A different approach by Ovchinnikov and Sigal can be found in [25]. In both publications the authors give an analytical form for the scaling function $s(t)$. We are going to use this result later on in section 6.4. We want to mention here that the results by Raphaël and Rodnianski cover all homotopy classes of the equivariant Wave Map. The singularity formation for higher homotopy classes was already studied by Rodnianski and Sterbenz in [30].

Extrinsic Formulation. In the later numerical simulations, we will use the extrinsic formulation, where we use Cartesian coordinates in the Euclidean space to avoid coordinate singularities. We write for the Wave Map:

$$U : \mathbb{M}^{2+1} \rightarrow \mathbb{S}^2 \hookrightarrow \mathbb{R}^3 \\ x \mapsto (U^1(t, x, y), U^2(t, x, y), U^3(t, x, y)).$$

The line element simply is

$$ds_{\mathbb{R}^3}^2 = (dU^1)^2 + (dU^2)^2 + (dU^3)^2.$$

The field equations, consisting of the equations of motion and the constraint equation, take the form:

$$(10) \quad \square_g U^A - 2\lambda U^A = 0,$$

$$(11) \quad U^A U_A - 1 = 0.$$

The Lagrangian parameter $\lambda = \lambda(t, x, y)$ can be computed by multiplying the equation of motion (10) with u_A and the use of the constraint equation (11) and its derivative. This leads to

$$\lambda = -\frac{1}{2} (\nabla^a U^B \nabla_a U_B).$$

The resulting non-linear wave equation has the constraint condition already imprinted

$$\square_g U^A + (\nabla^a U^B \nabla_a U_B) U^A = 0.$$

Now, we also introduce Cartesian coordinates on the base manifold \mathbb{M}^{2+1}

$$ds_{\mathbb{M}^{2+1}}^2 = dt^2 - dx^2 - dy^2.$$

By the relabelling $u := U^1$, $v := U^2$ and $w := U^3$ we can write the equations (10) and (11) in the explicit form

$$(12) \quad \ddot{u} - \partial_{xx}u - \partial_{yy}u - 2\lambda u = 0,$$

$$(13) \quad \ddot{v} - \partial_{xx}v - \partial_{yy}v - 2\lambda v = 0,$$

$$(14) \quad \ddot{w} - \partial_{xx}w - \partial_{yy}w - 2\lambda w = 0,$$

$$(15) \quad \phi(u, v, w) = u^2 + v^2 + w^2 - 1 \equiv 0.$$

The Lagrangian multiplier is given explicitly by

$$(16) \quad \lambda = -\frac{1}{2} \left[\dot{u}^2 + \dot{v}^2 + \dot{w}^2 - (\partial_x u)^2 - (\partial_x v)^2 - (\partial_x w)^2 - (\partial_y u)^2 - (\partial_y v)^2 - (\partial_y w)^2 \right]$$

The hidden constraint for the velocities is the time derivative of (15):

$$(17) \quad \psi(u, v, w, \dot{u}, \dot{v}, \dot{w}) = 2u\dot{u} + 2v\dot{v} + 2w\dot{w} \equiv 0.$$

We use the following relation between the intrinsic and extrinsic formulation:

$$(18) \quad u = \sin \vartheta \cos \varphi$$

$$(19) \quad v = \sin \vartheta \sin \varphi$$

$$(20) \quad w = \cos \vartheta.$$

Now, we can use these relations to write the static solutions (8) in the extrinsic formulation

$$(21) \quad u_S(x, y) = \frac{2x}{1+r^2}, \quad v_S(x, y) = \frac{2y}{1+r^2}, \quad w_S(x, y) = w_S(r) = \pm \frac{1-r^2}{1+r^2},$$

with the radial coordinate $r = \sqrt{x^2 + y^2}$. The \pm sign in the expression for $w_S(x, y)$ corresponds to the \pm sign in (8). It is easy to see that the static solutions, which are maps from \mathbb{R}^2 into S^2 , are exactly the stereographic projections from the south (+) and the north (−) poles, respectively.

In conjecture 3 the existence of a scaling function $s(t)$ is mentioned with the property to rescale the static solution in a way to approximate the dynamical solution around the origin. We can determine the scale factor at every fixed time as follows: we choose the component function $w(t, r)$ of the Wave Map and choose $s(t)$ in such a way that the second radial derivatives at the origin of the static and the rescaled dynamical solution (21) agree³. We use the function $w_S(r)$ with the + sign because we prescribe initial data in such a way that the stereographic projection from the south pole is singled out. The scaling relationship

$$w_S(r) = w(t, s(t)r)$$

is assumed to be valid in a neighbourhood of the origin. Taking the second radial derivative and evaluating at the origin gives

$$w_S''(0) = s(t)^2 \partial_{rr} w(t, 0),$$

from which we can determine the scaling factor as

$$(22) \quad s(t) = \frac{2}{\sqrt{|\partial_{rr} w(t, 0)|}}.$$

4. ENERGY CONSERVATION

From (3) we can get the energy-momentum tensor by variation of the action with respect to the inverse metric g^{ab} of the base space \mathcal{M} :

$$(23) \quad T_{ab} = \nabla_a U^A \nabla_b U^B \delta_{AB} - \frac{1}{2} \nabla_c U^A \nabla^c U^B \delta_{AB} g_{ab} - \lambda \phi g_{ab}$$

³In [5] the first derivatives are used to compute the scaling function. But in the extrinsic formulation the function w_S of the static solution is an even function and thus has vanishing odd derivatives at the origin.

In general, the energy of a matter field on a spatial slice in \mathcal{M} as measured by an observer field with 4-velocity t^a is defined by

$$E(t) = \frac{1}{2} \int_{\Sigma_t} t^a n^b T_{ab} \sqrt{|\gamma|} d^m x.$$

The slicing of the manifold \mathcal{M} implies a (negative definite) spatial metric γ_{ab} on the slice Σ_t , which has the future-pointing normal vector field n^b . For our purposes it is enough to consider flat space-like hyper-planes Σ_t . Furthermore, we choose static observers so that $t^a = (1, 0, 0) = n^a$. This and the energy-momentum tensor (23) lead to the following form of the energy contained inside a spatial domain $\Omega \subseteq \mathbb{R}^2$

$$E_\phi(t) = \frac{1}{2} \int_{\Omega} [\dot{U}^A \dot{U}_A + \partial_x U^A \partial_x U_A + \partial_y U^A \partial_y U_A - \lambda \phi(U)] dx dy.$$

Here we write E_ϕ in order to indicate that we do not necessarily impose the constraint. This has the consequence that the Energy-Momentum tensor is not divergence-free, as we find by computing its divergence

$$(24) \quad \nabla^a T_{ab} = -(\partial_b \lambda) \phi.$$

From (24) we can see clearly that the energy-momentum tensor is divergence free, provided $\phi = 0$, i.e., if and only if the constraint is satisfied. But what will happen if this is not the case? This is what almost invariably happens in a numerical simulation. We can use the above formula to find the energy loss due to the constraint violation.

We need the projection of (24) along the (constant) time-like vector t^a

$$(25) \quad t^b \nabla^a T_{ab} = -\left(t^b \partial_b \lambda\right) \phi.$$

We can interpret this equation as a continuity equation with an additional source on the right hand side. Using the fact that we are working on Minkowski space-time in Cartesian coordinates, we write for (25) with a dot as the time derivative

$$(26) \quad \dot{T}_{00} + \partial^k T_{0k} = -\dot{\lambda} \phi$$

where small Latin indices from the middle of the alphabet denote the spatial coordinates of the Minkowski spacetime.

The required components of the energy-momentum tensor are

$$(27) \quad \begin{aligned} T_{00} &= \frac{1}{2} \dot{U}^A \dot{U}_A - \frac{1}{2} \partial^k U^A \partial_k U_A - \lambda \phi =: \rho - \lambda \phi \\ T_{0k} &= \dot{U}^A \partial_k U_A =: j_k \end{aligned}$$

with the ‘true’ energy density ρ of the system when the constraint is satisfied and the momentum current density j_k . Now we can express (26) as

$$\begin{aligned} \dot{\rho} - \dot{\lambda} \phi - \lambda \dot{\phi} + \partial_k j^k &= -\dot{\lambda} \phi \\ \implies \dot{\rho} + \partial_k j^k &= \lambda \dot{\phi} \end{aligned}$$

and integrate over the domain Ω at a fixed time

$$\int_{\Omega} \dot{\rho} dx dy + \int_{\Omega} \partial_k j^k dx dy = \int_{\Omega} \lambda \dot{\phi} dx dy.$$

The first term on the left hand side in this equation is the time derivative of the ‘true’ energy E and the second term is an integral over the divergence of j_k . With the help of Gauss’ theorem, we can write the divergence term as a surface integral over the boundary $\partial\Omega$

$$(28) \quad \begin{aligned} \dot{E} + \int_{\partial\Omega} n_k j^k dS &= \int_{\Omega} \lambda \dot{\phi} dx dy \\ \implies \dot{E} &= \int_{\Omega} \lambda \dot{\phi} dx dy - \int_{\partial\Omega} n_k j^k dS \end{aligned}$$

with the normal vector field n_k on the boundary and the boundary element dS . The change of the energy between two instants of time is obtained by integrating over a time interval $[t_1, t_2]$

$$(29) \quad \Delta E = E(t_2) - E(t_1) = \int_{t_1}^{t_2} \int_{\Omega} \lambda \psi \, dt \, dx \, dy - \int_{t_1}^{t_2} \int_{\partial\Omega} n_k j^k \, dt \, dS.$$

The boundary term in (29) can be controlled by choosing appropriate boundary conditions. Inserting the definition of j^k we find for the integrand

$$(30) \quad n_k j^k \stackrel{(27)}{=} \dot{U}^A n^k \partial_k U_A.$$

In our numerical code we use homogeneous Neumann boundary conditions on all the unknowns U_A

$$n^k \partial_k U_A = 0.$$

With these boundary conditions the boundary term (30) vanishes and (29) reduces to

$$\Delta E = \int_{t_1}^{t_2} \int_{\Omega} \lambda \psi \, dt \, dx \, dy.$$

This is the change of the energy, which is due to the violation of the constraints. With other boundary conditions, for example Sommerfeld conditions, the boundary term would remain and describe an energy flux through the boundary.

5. NUMERICAL SETUP

5.1. Spatial Discretisation. In our investigations we use the Method of Lines approach for numerically solving PDEs. This means here we discretized the spatial variables with Finite Differences and evolve the resulting grid functions with either the fourth order Runge-Kutta or the Rattle method.

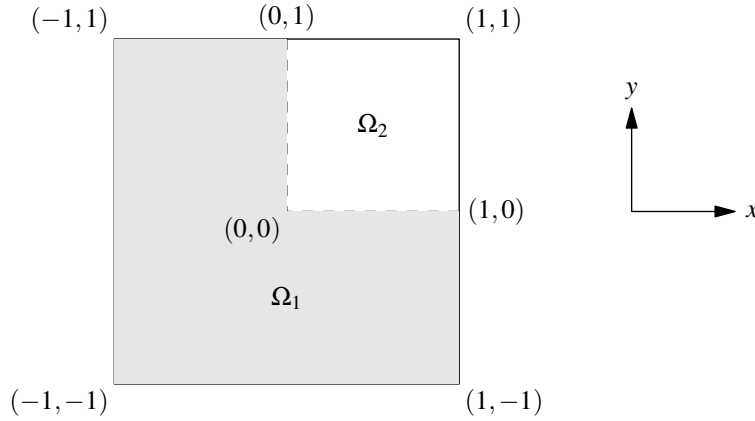


FIGURE 1. Domains of integration. Full domain $\Omega_1 = [-1, 1] \times [-1, 1]$ and the reduced (quarter) domain $\Omega_2 = [0, 1] \times [0, 1]$.

In section 6.1, 6.2 and 6.3 we are going to compare the results for the time integration methods directly. There, we perform our simulations on the domain of integration $\Omega_1 = [-1, 1] \times [-1, 1]$ (see figure 1) and discretize it via an equidistant grid.

$$\begin{aligned} x &\longrightarrow x_j = -1 + (j-1)h_x & j &= 1, \dots, N_x \\ y &\longrightarrow y_k = -1 + (k-1)h_y & k &= 1, \dots, N_y. \end{aligned}$$

with the grid spacings $h_x = x_{j+1} - x_j$ and $h_y = y_{k+1} - y_k$. All functions $f(x, y)$ will be evaluated on the grid nodes:

$$f(x, y) \longrightarrow f(x_j, y_k) = f_{j,k}.$$

This leads to approximations of the derivatives by differences of the function values at the grid points. For fourth order accuracy we write the following standard five point formulas for the derivative with respect to x at a point (j, k) :

$$\begin{aligned}\partial_x f|_{(j,k)} &= \frac{f_{j-2,k} - 8f_{j-1,k} + 8f_{j+1,k} - f_{j+2,k}}{12h_x}, \\ \partial_{xx} f|_{(j,k)} &= \frac{-f_{j-2,k} + 16f_{j-1,k} - 30f_{j,k} + 16f_{j+1,k} - f_{j+2,k}}{12h_x^2}.\end{aligned}$$

Derivatives with respect to y can be done equivalently. In all our computations we use the same grid spacing: $h_x = h_y$ in x and y directions.

For the simulations on the blow up dynamics in section 6.4, we use the symmetry of the system to reduce the domain of integration to a quarter of Ω_1 only. This has the advantage, that we effectively double the number of grid points with the same numerical costs. The new grid covers therefore the domain $\Omega_2 = [0, 1] \times [0, 1]$ (see also figure 1).

5.2. Boundary Conditions. As mentioned above, we use homogeneous Neumann conditions for the numerical calculations where we compare the Runge- Kutta and the Rattle method (this is important for the above described energy correction). We implement this boundary condition by imposing symmetries for the grid functions across the grid boundary. This gives us the possibility to determine the grid functions on points, which are beyond the boundaries (ghost points) which are needed for the evaluation of the finite difference operators. On the left boundary ($j = 1$) we get

$$f_{0,k} = f_{2,k} \quad \text{and} \quad f_{-1,k} = f_{3,k}$$

and on the right boundary ($j = N_x$)

$$f_{N_x+1,k} = f_{N_x-1,k} \quad \text{and} \quad f_{N_x+2,k} = f_{N_x-2,k}$$

and similarly we set the boundary conditions in the y direction.

The symmetries of the functions u and v make it necessary to impose different boundary conditions for the computations on the reduced domain Ω_2 . For the function u , we need along the boundary $x = 0$ and for the function v along $y = 0$ Dirichlet boundary conditions and not Neumann ones. On those boundaries, we have $u(0, y) = 0$ respectively $v(x, 0) = 0$. On the remaining three boundaries we can keep the Neumann conditions. To compute the ghost points for the Dirichlet boundary conditions we use the following relations on the left boundary

$$f_{0,k} = -f_{2,k} \quad \text{and} \quad f_{-1,k} = -f_{3,k}$$

The boundaries where we have to change the boundary conditions are for both functions left boundaries, therefore, we not need the equivalent relations on the right boundaries.

5.3. Initial data. The initial data we use are a polynomial bump with zeros at r_1 and r_2 :

$$(31) \quad \vartheta_0(r) = \begin{cases} A \left(4 \frac{(r-r_1)(r_2-r)}{(r_2-r_1)^2} \right)^n & \text{for } r \in [r_1, r_2] \\ 0 & \text{otherwise.} \end{cases}$$

The constant A represents the amplitude of $\vartheta_0(r)$. By using the relations (18), (19) and (20) we get the initial data for the extrinsic formulation. Throughout this article we use in all computations the parameters $r_1 = 0.5$, $r_2 = 1$ and $n = 4$. The initial data (31) describe a ring shaped bump in the xy -plane for the function $w(t, x, y)$ centred around the origin.

In order that the Cauchy problem is well posed we also need initial data for the velocities. We choose

$$\begin{aligned}\dot{u}(0, x, y) &= \partial_r u = \cos \vartheta_0(r) \vartheta_0'(r) \frac{x}{r} \\ \dot{v}(0, x, y) &= \partial_r v = \cos \vartheta_0(r) \vartheta_0'(r) \frac{y}{r} \\ \dot{w}(0, x, y) &= \partial_r w = -\sin \vartheta_0(r) \vartheta_0'(r).\end{aligned}$$

With this choice of initial data for the velocities, the above described ring shrinks towards the origin. This means that the energy concentrates around the origin. After the function $w(t, x, y)$ has reached a minimum close to the origin the ring starts expanding again. If the energy concentration at the origin is large enough, one expects a singularity formation like it is assumed in the three conjectures 1, 2, 3 above.

Raphaël and Rodnianski presented in [26] a set of initial data for analytical, but also numerical investigations. However we have chosen the initial data (31) to compare our *numerical* results with the ones in [5].

6. RESULTS

The main aim in this article is to compare the evolution of a constrained system by using an integration method for a free evolution and a method, which explicitly takes the constraint equations into account. As our model we choose the above described 2+1 dimensional Wave Map equations in the extrinsic formulation, as an example for a wave-like PDE system, which is constrained by additional (algebraic) conditions.

In the case of the free evolution we use the equations (12), (13), (14) and replace the Lagrangian multiplier λ with the expression (16). For this calculation we use the standard fourth order Runge-Kutta method (RK4). These results will be compared with the ones gained from the time evolution taking the constraint equation into account. Here we are going to use equations (12), (13), (14), (15) and (17). The time evolution will be done with the Rattle method (RTL) described in section 2. For the Rattle method we choose for the maximally allowed constraint violation the value 10^{-12} . This means that for all times t : $\|\phi\|_{\max}(t) \leq 10^{-12}$ as well as $\|\psi\|_{\max}(t) \leq 10^{-12}$, where $\|\cdot\|_{\max}$ is the maximum norm. If this accuracy cannot be reached within 100 iterations the program aborts. For the computations presented here this was never the case. All following computations are done in the time interval $t \in [0, 1.6]$ and with a Courant-Friedrichs-Lewy factor $\Delta t/h = 0.2$. In the simulations, where we compare the two integration methods, we have chosen the values for the amplitude A in a way that none of the two integration methods breaks down.

6.1. Constraint functions. One of the main points in this article is the preservation of the constraint (15) and its derivative (17). In figure 2 we compare the constraint violation for the two different integration methods. We see clearly that the Runge-Kutta method leads to a permanent increase of the constraint violation during the time evolution. The Rattle method always keeps the constraint violation below the previously set value 10^{-12} .

For the velocity constraint ψ we can see in figure 3 qualitatively the same results as for the constraint ϕ . But it is worth mentioning that the Rattle methods preserves the velocity constraint even a few orders better than requested.

The accelerated increase of the constraint violation for the Runge-Kutta method at $t \approx 0.8$ occurs at the moment when the wave packet is reflected at the origin. During this reflection process the spatial derivatives near the origin are very high. This also leads to a strong deviation of the function from its theoretically fixed value at the origin.

We mention here, that the convergence for both methods is of the expected order. If we rescale the results shown in figure 2 and 3 for different numerical resolutions with the expected, fourth order, convergence rate, the curves for the Runge-Kutta method cannot visually be distinguished. To check the convergence of the Rattle method, we cannot use the constraint preservation, because in this method we predefine the maximum of the constraint violation. However, by checking the convergence rate with the function w with the function w we also obtain the expected second order convergence.

6.2. Behaviour at the Origin. At the origin $r = 0$, respectively $(x = 0, y = 0)$ the solution $\vartheta(t, r)$ of the equivariant Wave Map equation (6) has the noteworthy feature that it is constant during the whole time evolution. One can show that from the equations that the solution evolving from our class of initial data necessarily satisfies for all t

$$\vartheta(t, 0) = 0 \quad \text{and respectively} \quad w(t, 0, 0) = 1.$$

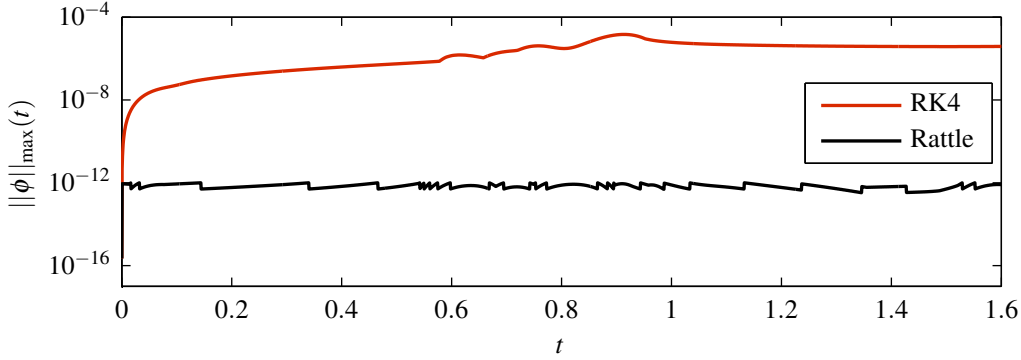


FIGURE 2. Maximum norm $\|\phi\|_{\max}(t)$ for the constraint ϕ during the time evolution for $A = 0.4$.

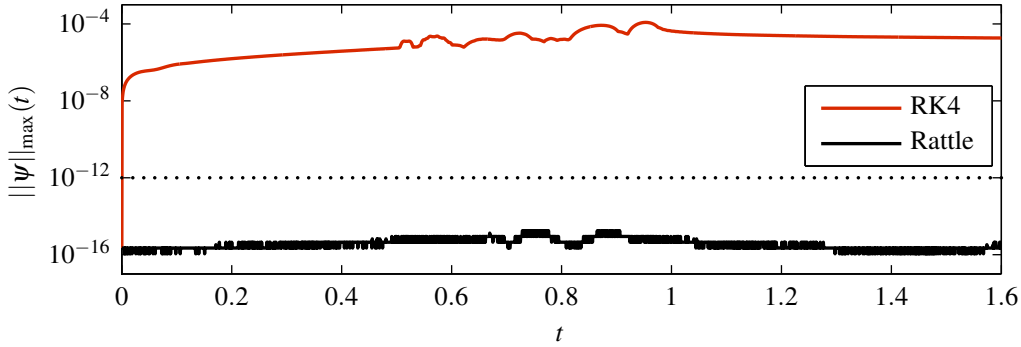


FIGURE 3. Maximum norm $\|\psi\|_{\max}(t)$ for the velocity constraint ψ during the time evolution for $A = 0.4$. The dotted line is the preset value for the maximum of the constraint violation.

This condition is not enforced in our code. In figure 4 we compare how the two integration methods preserve this property. We can see that the Rattle method always keeps the deviation $|w(t, 0, 0) - 1|$ under the predefined maximum of 10^{-12} for the constraint violation. As expected from the previous results, the Runge-Kutta method cannot preserve the property, because it lets the solution drift away from the constraint manifold. In the literature, this drift is a well known phenomenon for constrained ODEs (see [21]). Numerical solutions of constrained systems, in the formulation where the Lagrangian multipliers are eliminated, show this behaviour in general.

For larger values of A the Runge-Kutta method breaks down at the origin. This breakdown depends on the spatial resolution and is therefore a numerical phenomenon and not an indication for the collapse of the solution. The solution gained with the Rattle method shows a different behaviour. For large values of A the solution flips from $w(t, 0, 0) = 1$ to $w(t, 0, 0) = -1$. This indicates that it becomes increasingly difficult for the iterative algorithm of the constraint equation to find a solution and ultimately the iteration seems to approach the other static solution, the stereographic projection from the north pole, for which $w(t, 0, 0) = -1$. We take this behaviour as an indication that the solution is in the blow-up regime. For the critical value of the amplitude, we take the value where the behaviour at the origin changes and find $A^* \approx 0.81871173$.

6.3. Energy Conservation. An often used measure for the quality of numerical solutions of ODEs and PDEs is the energy conservation during the time evolution. Of course, this makes sense for non-dissipative systems only. We compare the energy conservation for the evolution computed with the Runge-Kutta and

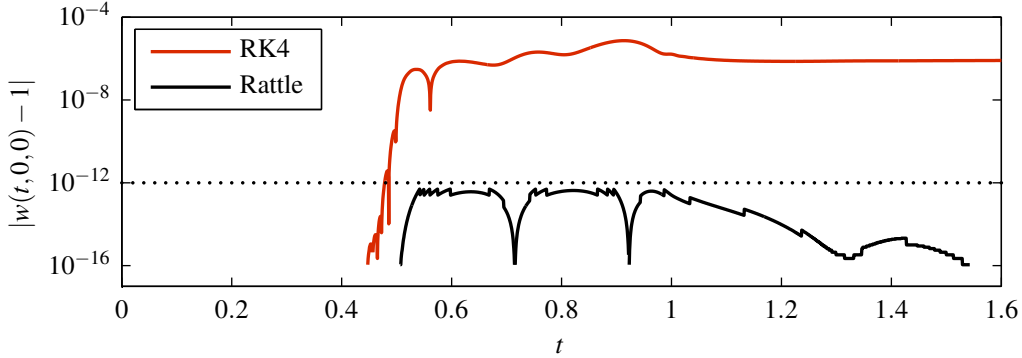


FIGURE 4. Displacement $|w(t, 0, 0) - 1|$ of the solution at the origin for $A = 0.4$ during the time evolution. The dotted line is the preset value for the maximum of the constraint violation.

the ones obtained with the Rattle method. We can see in figure 5 that the average energy conservation with the Rattle method is better than with the Runge-Kutta method.

In section 4 we presented the analytical formula for an energy loss, which is caused by the violation of the constraint equations. Our numerical investigations confirm the existence of this energy loss. We can use this term to correct the total energy $E_{\text{corr}} = E - \Delta E$. From figure 5 we see that the corrected energy is better preserved than without correction, and also in average better than with the Rattle method. Only during the reflection at the origin the Rattle method results in an better energy conservation.

The energy correction computed for the Rattle method is so small compared to the relative energy, that it can be neglected.

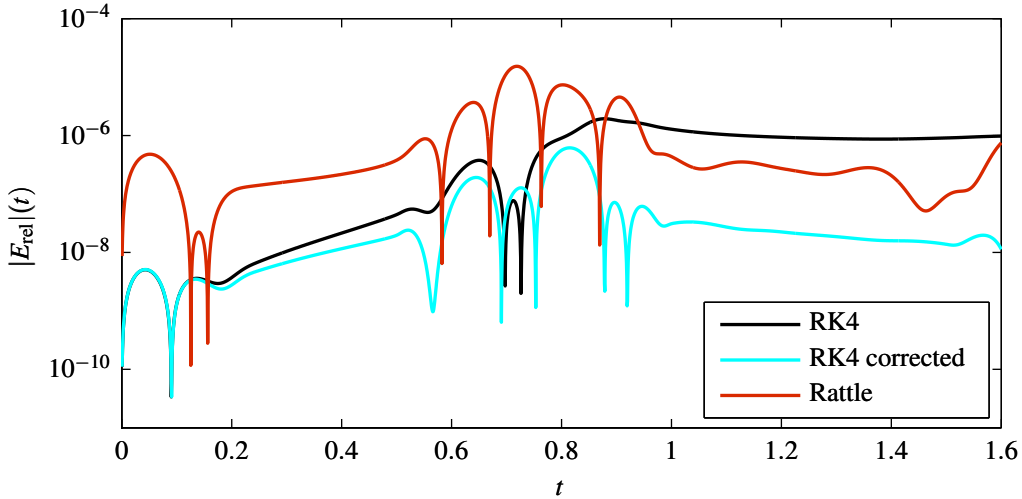


FIGURE 5. Relative energy $|E_{\text{rel}}|(t) = |1 - E(t)/E(0)|$ computed with the Runge-Kutta (corrected and uncorrected) and the Rattle methods for $A = 0.4$ and $N = 641$.

6.4. Scaling Function. The conjectures by Bizoń et.al. refer to the scaling function $s(t)$, which we determined in (22). This function plays a central role in the study of the singularity formation of Wave Maps [25, 26]. The importance comes from the fact, that with the help of $s(t)$ the dynamical solution can be rescaled in a way that it approximates the static solution during the singularity formation, around the point where the singularity will appear. This means the scaling function is directly involved in the blow-up. The

fact that the scaling function plays an crucial role in the singularity formation was shown by Struwe in [37]. The scaling function is an direct indicator for the shrinking of the static solution, which drives the singularity formation.

In this part we determine the scaling function for different values of the criticality parameter A in its dependence on time. All the calculations in this subsection have been performed with the Rattle method because of its superior behaviour in the critical regime. As mentioned before the simulations for this part were computed on the reduced domain of integration Ω_2 .

As we can see in figure 6, increasing the amplitude A towards the critical value A^* , the time interval in which the scaling function is approximately constant, increases. This means, that during this period the solution remains almost constant, hovering in a quasi-static state. But for higher resolutions this states last shorter. Therefore we are very confident the method we presented is able to deal with such critical situations, but the need for much higher resolutions is evident. We interpret this quasi-static state as the fact that the numerical scheme cannot follow the shrinking of the harmonic map anymore. Therefore for this numerical resolution the critical situation occurred. When the scaling function increases again, the resolution is again sufficient to follow this process.

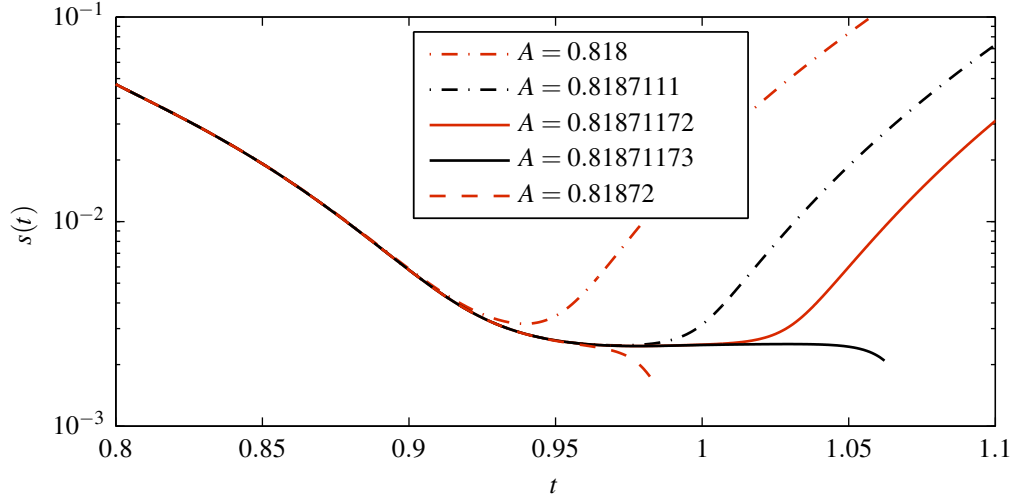


FIGURE 6. The scaling function $s(t)$ for different parameter values A . The value $A^* = 0.81871173$ is the critical amplitude.

In figure 7 we can see the scaling function $s(t)$ for different values of the amplitude parameter A . The black curve is the fit to the curve for the amplitude $A = 0.81871172$, which is the one closest to the critical value A^* . The interval $t \in [0.836, 0.85]$ between the dotted lines is the domain used for the fitting procedure. The fit was done with respect to the analytic expression

$$s(t) = \frac{1.04}{e} (T - t) \exp\left(-\sqrt{-\ln(T - t) + b}\right)$$

which is taken from [25]. The parameter b depends on the choice of the initial data. Our choice for the interval for the fit is a compromise between being close enough to the blow up time and the domain where we can be sure, that the scaling function numerically converges. The results presented here were computed with $N = 641$ grid points in x and y direction. For higher resolutions the amplitude $A^* = 0.81871173$ is not critical at all. The results of the fit were $T = 0.94151363$ and $b = -2.02978334$ with a residual error of $1.31486579 \cdot 10^{-8}$. The fit parameter were computed with the MATLAB function `lsqcurvefit` from the Optimization Toolbox.

Figure 8 shows the rescaled function $w(t, r/s(t))$ at different times and the static solution $w_S(r)$. The amplitude is $A = 0.81871172$, very close to the critical value $A^* = 0.81871173$. At $t = 0.919375$ the

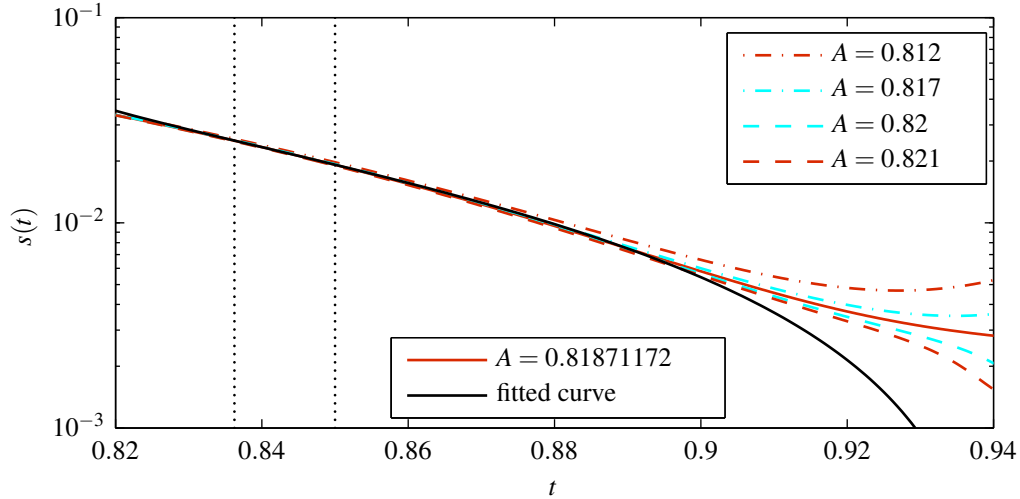


FIGURE 7. Fit of the scaling function $s(t)$ to the analytical expression, given in [25]. The computed blow up is $T = 0.94151363$. The value $A = 0.81871172$ is the last under-critical value shown, i.e., for which the solution does not change its behaviour at the origin.

solution reaches its overall minimum value of $w = -0.91372693$. Before this time the wave packet moves towards the origin, where it is reflected and subsequently moves away from the origin. We can see that the rescaled dynamic solution is approximated very well by the static solution near the origin. As mentioned before for larger amplitudes the solutions show a flip of the solution at the origin. In the caption of figure 5 in [5], Bizoń et. al. note the fact that the solution overshoots the value $-\pi$, which they consider as a necessary and sufficient condition for the blow up. We believe that in our case it is the observed flip at the origin, which indicates the same phenomenon.

7. CONCLUSION

In this article we demonstrated that the Rattle method can be very useful for the numerical time evolution of relativistic field equations. In terms of constraint conservation it is, by construction, superior compared to a free evolution scheme like the standard fourth order Runge-Kutta method. The usage of the constraint equations also leads to a more accurate behaviour in extreme situations, like we showed it for the behaviour of the Wave Map solution at the origin. At this point the solution should always take the same value. The Rattle method preserves this symmetry in the accuracy previously set as the limit of the constraint violation. The Runge-Kutta method leads to a drift away from this state.

We presented an energy correction term, which is a direct consequence of the constraint violation. The explicit computation of this deviation was used to correct the total energy. This energy deviation depends on the magnitude of the constraint violation, which is the reason why it can be ignored with the Rattle method by choosing the allowed constraint violation small enough. For the Runge-Kutta method it was possible to correct the energy in a way that the energy conservation during the whole time evolution is better than for the Rattle method. But this better energy conservation does not cure the other shortcomings namely the increasing constraint violation and violation of the symmetry at the origin.

Finally we presented some results obtained in the equivariant case using the Rattle method. We computed the scaling function $s(t)$ for different values for the amplitude and confirmed the expected behaviour that the rescaled dynamic solution approximates the static solution as the parameter A approaches a critical value. Since we obtain this behaviour without imposing the equivariance explicitly, this shows that the critical behaviour observed in the 1+1 codes is in fact stable under small non-spherical perturbations, which are inadvertently introduced due to the numerical errors. To our knowledge it has not been shown numerically

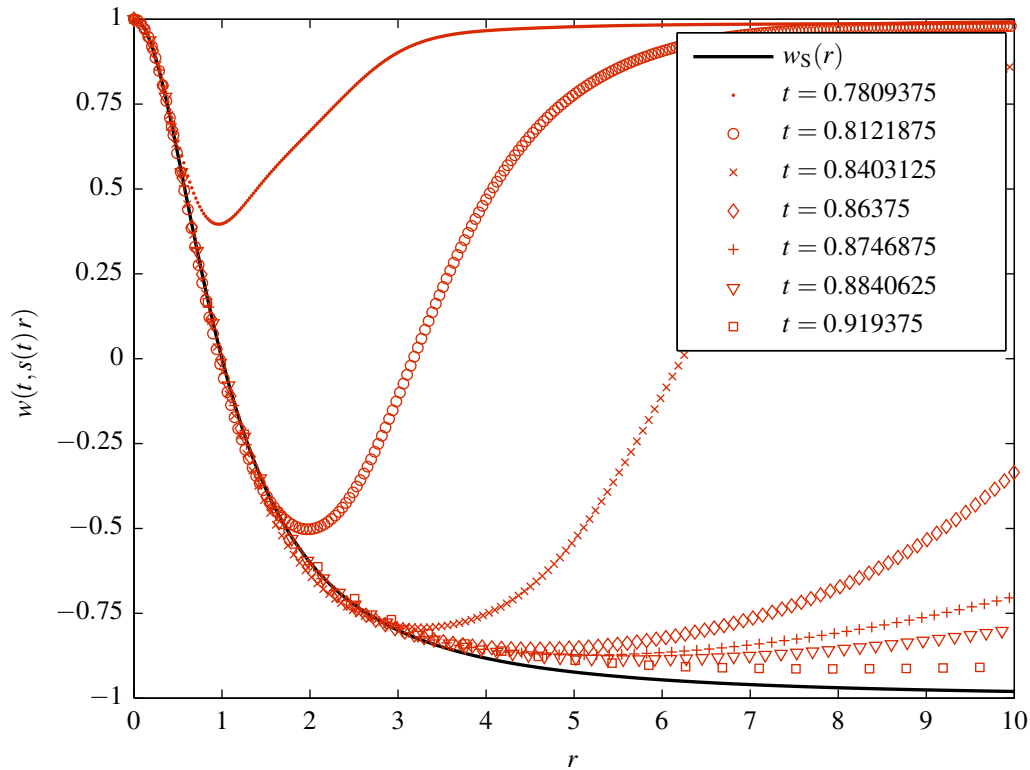


FIGURE 8. Ingoing wave packet for $A = 0.81871172$ rescaled with the scaling function $s(t)$ for various values of t . The rescaled functions $w(t, s(t)r)$ approximate the static solution $w_S(r)$. The function $w(t, r)$ reaches its minimum at $t = 0.919375$. The computation was done with $N = 641$ grid points on the quarter grid.

that critical behaviour will also appear in the non-equivariant case. In a future article, we are going to show that under explicit violation of the equivariance, we still observe the critical behaviour.

It is obvious from our results, that for an insight into the delicate details of the blow up dynamics much higher numerical resolutions are required. These could be achieved by using grid refinement techniques for example. However, the Rattle method applied to the extrinsic formulation of the 2+1 Wave Map seems to be a promising way to study this system without running into problems with coordinate singularities.

REFERENCES

- [1] H. C. Andersen, *Rattle: A “Velocity” Version of the Shake Algorithm for Molecular Dynamics Calculations*, J. Comput. Phys. **52** (1983), no. 1, 24–34.
- [2] B. K. Berger and P. T. Chruściel, *On “Asymptotically Flat” Space-Times with G_2 -Invariant Cauchy Surfaces*, Ann. Phys. **237** (1995), no. 2, 322–354.
- [3] B. K. Berger, D. Garfinkle, and E. Strasser, *New algorithm for Mixmaster dynamics*, Class. Quantum Grav. **14** (1997), no. 2, L29–L36.
- [4] B. K. Berger and V. Moncrief, *Numerical investigation of cosmological singularities*, Phys. Rev. D **48** (1993), no. 10, 4676–4688.
- [5] P. Bizoń, T. Chmaj, and Z. Tabor, *Formation of singularities for equivariant (2+1)- dimensional wave maps into the 2-sphere*, Nonlinearity **14** (2001), no. 5, 1041–1053.
- [6] D. Christodoulou and A. S. Tahvildar-Zadeh, *On the Regularity of Spherically Symmetric Wave Maps*, Comm. Pure Appl. Math. **46** (1993), no. 7, 1041–1091.
- [7] ———, *On the asymptotic behavior of spherically symmetric wave maps*, Duke Math. J. **71** (1993), no. 1, 31–69.
- [8] J. Frauendiener, *The applicability of constrained symplectic integrators in general relativity*, J. Phys. A **41** (2008), no. 38, 382005.

- [9] E. Hairer, C. Lubich, and G. Wanner, *Geometric numerical integration illustrated by the Störmer-Verlet method*, Acta Numer. (2003), 399–450.
- [10] ———, *Geometric Numerical Integration*, 2nd ed., Springer, 2006.
- [11] J. Isenberg and S. L. Liebling, *Singularity formation in 2+1 wave maps*, J. Math. Phys. **43** (2002), no. 1, 678–683.
- [12] S. V. Ketov, *Nonlinear Sigma model* (2009). online article on Scholarpedia: http://www.scholarpedia.org/article/Nonlinear_Sigma_model.
- [13] S. Klainerman and M. Machedon, *Space-time estimates for null forms and the local existence theorem*, Comm. Pure Appl. Math. **46** (1993), no. 12, 1221–1268.
- [14] S. Klainerman and I. Rodnianski, *On the Global Regularity of Wave Maps in the Critical Sobolev Norm*, Int. Math. Res. Not. IMRS **2001** (2001), no. 13, 655–677.
- [15] S. Klainerman and S. Selberg, *Remark on the optimal regularity for equations of wave maps type*, Comm. Partial Differential Equations **22** (1997), no. 5–6, 901–918.
- [16] J. Krieger, *Global Regularity of Wave Maps from R^{3+1} to Surfaces*, Comm. Math. Phys. **238** (2003), no. 1–2, 333–366.
- [17] ———, *Global Regularity of Wave Maps from R^{2+1} to H^2 . Small Energy*, Comm. Math. Phys. **250** (2004), no. 3, 507–580.
- [18] J. Krieger, *Global Regularity and Singularity Development for Wave Maps*, Geometric Flows, 2008.
- [19] J. Krieger, W. Schlag, and D. Tataru, *Renormalization and blow up for charge one equivariant critical wave maps*, Invent. Math. **171** (2008), no. 3, 543–615.
- [20] J. Krieger and W. Schlag, *Concentration Compactness for Critical Wave Maps* (2009). preprint available at: [arXiv:0908.2474v1](https://arxiv.org/abs/0908.2474v1).
- [21] B. Leimkuhler and S. Reich, *Simulating Hamiltonian Dynamics*, 1st ed., Cambridge University Press, 2004.
- [22] B. J. Leimkuhler and R. D. Skeel, *Symplectic Numerical Integrators in Constrained Hamiltonian Systems*, J. Comput. Phys. **112** (1994), no. 1, 117–125.
- [23] C. Lubich, B. Walther, and B. Brüggemann, *Symplectic integration of post-Newtonian equations of motion with spin*, Phys. Rev. D **81** (2010), no. 10, 104025.
- [24] R. I. McLachlan and G. R. W. Quispel, *Geometric Integrators for ODEs*, J. Phys. A **39** (2006), no. 19, 5251–5285.
- [25] Yu. N. Ovchinnikov and I. M. Sigal, *On Collapse of Wave Maps*, Physica D **240** (2011), no. 17, 1311–1324.
- [26] P. Raphaël and I. Rodnianski, *Stable Blow Up Dynamics for the Critical Corotational Wave Maps and Equivariant Yang-Mills Problems* (2009). preprint on [arXiv.org:0911.0692](https://arxiv.org/abs/0911.0692).
- [27] R. Richter and C. Lubich, *Free and constrained symplectic integrators for numerical general relativity*, Class. Quantum Grav. **25** (2008), no. 22, 225018.
- [28] R. Richter, *Strongly hyperbolic Hamiltonian systems in numerical relativity: formulation and symplectic integration*, Class. Quantum Grav. **26** (2009), no. 14, 145017.
- [29] H. Ringström, *On a Wave Map Equation Arising in General Relativity*, Comm. Pure Appl. Math. **57** (2004), no. 5, 657–703.
- [30] I. Rodnianski and J. Sterbenz, *On the Formation of Singularities in the Critical $O(3)$ σ -Model* (2008). preprint on [arXiv:math/0605023v3](https://arxiv.org/abs/math/0605023v3).
- [31] J.-P. Ryckaert, G. Ciccotti, and H. J. C. Berendsen, *Numerical Integration of the Cartesian Equations of Motion of a System with Constraints: Molecular Dynamics of n-Alkanes*, J. Comput. Phys. **23** (1977), no. 3, 327–341.
- [32] J. Shatah and M. Struwe, *Geometric Wave Equations*, 1st ed., Courant Institute of Mathematical Science/American Mathematical Society, 2000.
- [33] ———, *The Cauchy Problem for Wave Maps*, International Mathematics Research Notices **2002** (2002), no. 11, 555–572.
- [34] J. Shatah and A. S. Tahvildar-Zadeh, *On the Cauchy Problem for Equivariant Wave Maps*, Comm. Pure Appl. Math. **47** (1994), no. 5, 719–754.
- [35] M. Struwe, *Radially symmetric wave maps from $(1+2)$ -dimensional Minkowski space to the sphere*, Math. Z. **242** (2002), no. 3, 407–414.
- [36] ———, *Radially symmetric wave maps from $(1+2)$ -dimensional Minkowski space to general targets*, Calc. Var. Partial Differential Equations **16** (2003), no. 4, 431–437.
- [37] ———, *Equivariant Wave Maps in Two Space Dimensions – To the memory of Professor Jürgen Moser*, Comm. Pure Appl. Math. **56** (2003), no. 7, 0815–0823.
- [38] J. Sterbenz and D. Tataru, *Energy Dispersed Large Data Wave Maps in 2+1 Dimensions*, Comm. Math. Phys. **298** (2010), no. 1, 139–230.
- [39] ———, *Regularity of Wave Maps in Dimension 2+1*, Comm. Math. Phys. **298** (2010), no. 1, 231–264.
- [40] T. Tao, *Global regularity of wave maps, I: small critical Sobolev norm in high dimension*, Int. Math. Res. Not. IMRN **2001** (2001), no. 6, 299–328.
- [41] ———, *Global Regularity of Wave Maps II. Small Energy in Two Dimensions*, Comm. Math. Phys. **224** (2001), no. 2, 443–544.
- [42] D. Tataru, *Local and global results for wave maps I*, Comm. Partial Differential Equations **23** (1998), no. 9–10, 1781–1793.
- [43] ———, *The Wave Maps Equation*, Bull. Amer. Math. Soc. **41** (2004), no. 2, 185–204.
- [44] ———, *Rough Solutions for the Wave Maps Equation*, Amer. J. Math. **127** (2005), no. 2, 293–377.

DEPARTMENT FOR MATHEMATICS AND STATISTICS, UNIVERSITY OF OTAGO, PO BOX 56, DUNEDIN 9054, NEW ZEALAND

E-mail address: rpeter@maths.otago.ac.nz

E-mail address: joergf@maths.otago.ac.nz